Journal of Applied Physics

Magnetic and magnetoelectric response of Gd doped nickel ferrite and barium titanate nanocomposites

Cite as: J. Appl. Phys. **127**, 114104 (2020); https://doi.org/10.1063/1.5138239
Submitted: 14 November 2019 . Accepted: 02 March 2020 . Published Online: 18 March 2020

Tripta Parida, Amritesh Kumar, B. S. Murty, and G. Markandeyulu

Journal of Applied Physics ARTICLE scitation.org/journal/jap

Magnetic and magnetoelectric response of Gd doped nickel ferrite and barium titanate nanocomposites

Cite as: J. Appl. Phys. **127**, 114104 (2020); doi: 10.1063/1.5138239
Submitted: 14 November 2019 · Accepted: 2 March 2020 ·
Published Online: 18 March 2020

Tripta Parida,[1] Amritesh Kumar,[2] B. S. Murty,[3] and G. Markandeyulu[1,a)]

AFFILIATIONS

[1]Department of Physics, Indian Institute of Technology Madras, Chennai 600036, India
[2]Department of Applied Mechanics, Indian Institute of Technology Madras, Chennai 600036, India
[3]Department of Metallurgical and Materials Engineering, Indian Institute of Technology Madras, Chennai 600036, India

[a)]**Author to whom correspondence should be addressed:** mark@iitm.ac.in. **Tel.:** +91-44-22574870

ABSTRACT

Composites of $NiFe_2O_4$ (NFO)–$BaTiO_3$ (BTO) and $NiGd_{0.01}Fe_{1.99}O_4$ (G0.01)–BTO were investigated by x-ray diffraction, magnetization, transmission electron microscopy, magnetocapacitance, and ferroelectric studies. NFO and G0.01 nanoparticles were synthesized by the sol-gel method. The crystallite size of the nanoparticles estimated from the x-ray diffraction patterns is 20–22 nm. The average crystallite sizes of NFO and G0.01 nanoparticles were estimated from the transmission electron micrographs as 26 (1) nm and 22.3 (0.3) nm, respectively. These nanoparticles were encapsulated in a BTO shell, resulting in the formation of nanocomposites. Room temperature magnetization (at 60 kOe) of G0.01 nanoparticles was found to be slightly higher than that of NFO nanoparticles, due to the larger moment of Gd^{3+} than that of Fe^{3+}. Also, the magnetization of G0.01–BTO is more than that of NFO–BTO nanocomposites. The magnetoelectric effect was observed with a magnetocapacitance value of approximately −10% at 10 kHz in both the composites.

I. INTRODUCTION

The research to obtain miniaturized devices using the functional properties of nanomaterials is of topical interest in recent times. One such property, the magnetoelectric (ME) response, is reported to arise due to the strain mediated effect, which is a result of the combination of the magnetostrictive effect of the magnetic phase and the piezoelectric effect of the ferroelectric phase. Toward this, materials exhibiting the ME effect have found various applications in the interdisciplinary fields of biomedical engineering and electronics.[1,2] These are useful in a wide range of applications starting from thin film devices such as ME actuators, sensors, etc., to the memory devices as well as carrier materials for drug delivery.[3]

Bharathi *et al.* have reported that rare-earth doped nickel ferrite compounds exhibited ferroelectricity and magnetocapacitance (MC %) of −4% in Dy and −3% in Gd doped NFO with a magnetoelectric voltage coefficient (MEVC) in the range of 1.5–2 mV/cm Oe.[4,5]

The ME coupling phenomenon in the composite system of NFO–BTO was first observed in the 1970s by Boomgaard *et al.*[6] 0–3 particulate composites have been reported to exhibit low MEVC values as predicted from theory, due to factors such as the following:[7]

1. The difference in thermal expansions of piezoelectric and ferrite phases leads to misfit strain at the interface, thereby reducing the densification.
2. Strain transfer between piezoelectric and magnetostrictive phases weakens due to the secondary phase formation from chemical reactions between these phases during high temperature sintering.
3. Leakage current due to low resistivity ($\sim 10^7\ \Omega$ cm)[8] of the magnetic phase compared to that ($10^{12}\ \Omega$ cm)[9] of the ferroelectric phase.

In order to reduce the contact area between the ferrite particles, core–shell composites with a piezoelectric material such as BTO as the shell have been prepared.[10,11] Zhou *et al.*[12] have reported the ME effect (12 mV/cm Oe) in NFO–BTO core–shell composites produced by a simple hydrothermal method. NFO nanoparticles were synthesized followed by the shell formation of BTO. Banerjee *et al.*[13] have

reported a self-assembly of NFO–BTO core–shell composites using DNA functionalized nanoparticles. Raidongia *et al.*[11] have synthesized CFO–BTO core–shell nanoparticles and nanotubes using a combination of solution processing and high temperature calcination. Chaudhuri and Mandal[14] have reported that MEVC of the CFO–BTO (1:1) core–shell was 35 times higher than that of the CFO–BTO (1:1) mixture.

Based on the observation of the structural distortion driven ME effect in Gd doped NFO[15] and the reports on CFO/NFO–BTO core–shell composites, core–shell nanostructures of Gd doped NFO as a magnetic phase and BTO as a piezoelectric phase were prepared. The physical and structural properties of G0.01–BTO are compared with those of NFO–BTO core shell nanocomposites, in this study.

II. EXPERIMENTAL DETAILS

NFO and G0.01 nanoparticles were synthesized by the sol-gel method. Stoichiometric amounts of the corresponding metal nitrates were dissolved in ethylene glycol, and using triethyl amine as a catalyst, as reported.[16] 0.1 g of citric acid was added to 0.029 g of barium carbonate ($BaCO_3$) to form Ba citrate solution. 1 g citric acid was added to titanium iso-propoxide $[Ti(OCH(CH_3)_2)_4]$ in the ethanol medium in a separate container to obtain Ti citrate solution. Both these solutions were mixed to form equimolar Ba and Ti citrate solutions. 0.1 g of NFO and G0.01 nanoparticles were mixed in Ba and Ti citrate solutions, and this mixture was sonicated for 2 h and was dried at 60 °C to obtain the powders, which were heat treated at 750 °C for 5 h.[17] Powder x-ray diffraction (XRD) patterns collected employing a PANalytical X'Pert PRO diffractometer using Cu K_α radiation confirmed the formation of NFO/G0.01 in a spinel structure and BTO in a perovskite structure. Dark-field TEM images and selected area diffraction patterns of the nanoparticles were captured using a TECNAI T20 electron microscope operating at an applied voltage of 200 kV. The images and line profile analysis obtained by high-angle annular dark-field scanning transmission electron microscopy (HAADF-STEM) employing FEI Titan G2 60-300 clearly reveal the core shell structures of G0.01–BTO composites.

A VSM with a SQUID detector (SVSM MPMS 3, QD, USA) was employed to carry out magnetization measurements. Magnetocapacitance measurements on green compacts of NFO–BTO and G0.01–BTO nanocomposites were carried out by employing an HP 4192A impedance analyzer, at a frequency of 10 kHz, in magnetic fields up to 0.7 T applied along and perpendicular to the axis of the (disk shaped) sample. Magnetoelectric measurements were also carried out on the same samples using an ME measurement setup (details of the experimental setup are mentioned in Ref. 18). Input signals for both the ac and dc fields were generated by the function generator. A sinusoidal AC signal at a constant frequency of 1 kHz was amplified by an amplifier (KEPCO, BOP 36-6DL). To measure the voltage generated across the piezoelectric material, contacts were given on the top and bottom surfaces of the sample and were connected to a lock-in-amplifier (DSP7265).

III. RESULTS AND DISCUSSION

Powder x-ray diffraction (XRD) patterns shown in Figs. 1(a) and 1(b) confirm the formation of NFO and G0.01 nanoparticles. Rietveld refinement was carried out, and χ^2 values were observed to be 1.19 and 1.10 for NFO and G0.01, respectively.

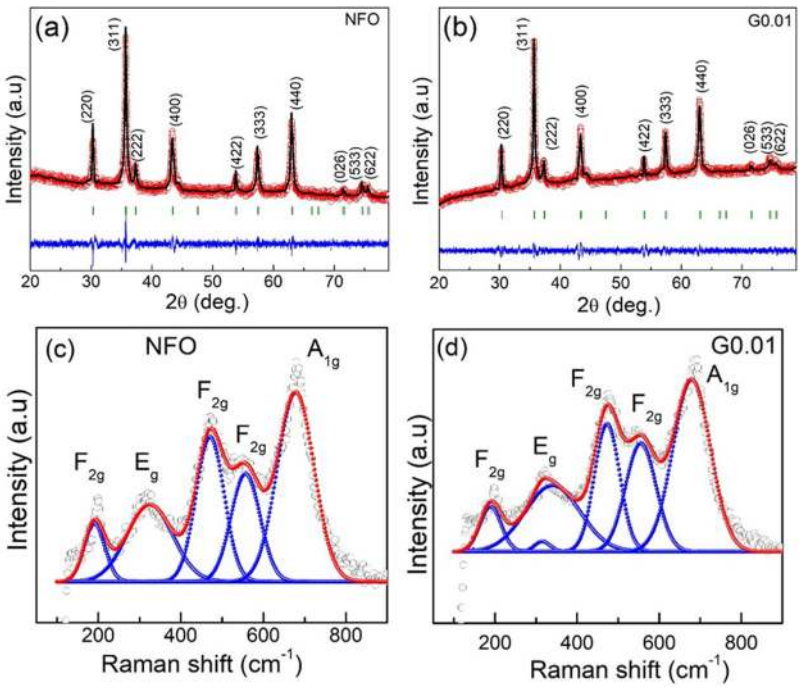

FIG. 1. Powder x-ray diffraction pattern on (a) NFO and (b) G0.01 as synthesized nanoparticles and Raman spectra for (c) NFO and (d) G0.01 nanoparticles.

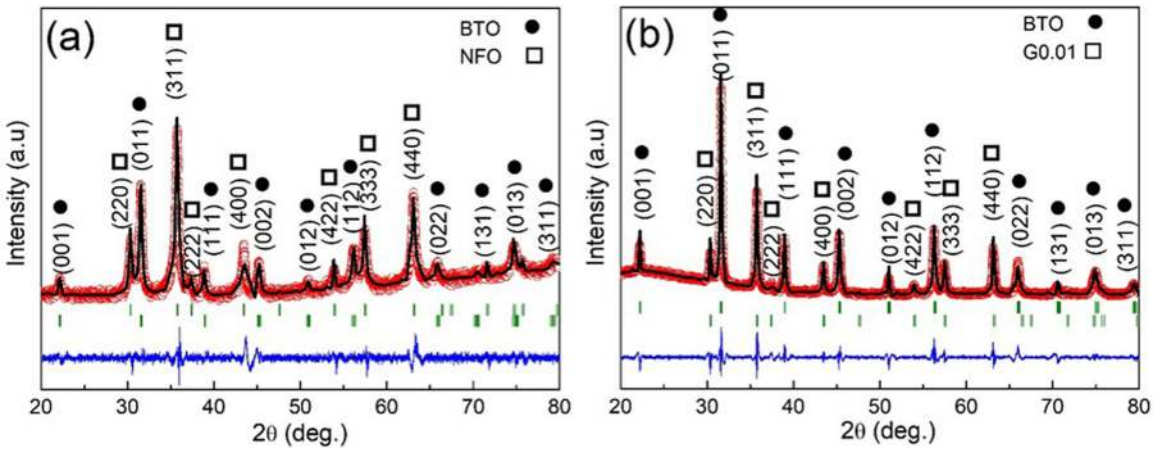

FIG. 2. Powder x-ray diffraction pattern of (a) NFO–BTO and (b) G0.01–BTO nanocomposites.

The average crystallite size was estimated to be 20 nm for NFO and 22 nm for G0.01 nanoparticles by the Williamson–Hall method. The lattice parameters of NFO and G0.01 calculated from Reitveld analysis are 8.341 (0.001) Å and 8.339 (0.001) Å, respectively. Since the concentration of Gd is low, XRD analysis could not reveal a perceptible change in the lattice parameter. Figures 1(c) and 1(d) show the Raman spectra for NFO and G0.01 nanoparticles, respectively. There are five Raman active modes in ferrites, viz., one each of A_{1g}, E_g, and $3T_{2g}$.[19] The A_{1g} mode (at 702 cm^{-1}) can be attributed to the symmetric stretching of the metal (tetrahedral site)–oxygen (Ni–O and Fe–O) bonds, and the E_g mode (at 333 cm^{-1}) is due to the symmetric bending of the metal (octahedral site)–oxygen bonds. Peaks at 212, 482, and 577 cm^{-1} correspond to the $3T_{2g}$ mode. The E_g mode peak is seen to split into two as shown in Fig. 1(d), which is an indication of the presence of Gd^{3+} at the octahedral site.

XRD patterns of the nanocomposites are shown in Fig. 2 where the phases corresponding to NFO and G0.01 are indicated by □ and those corresponding to BTO by ●; the phase percentages

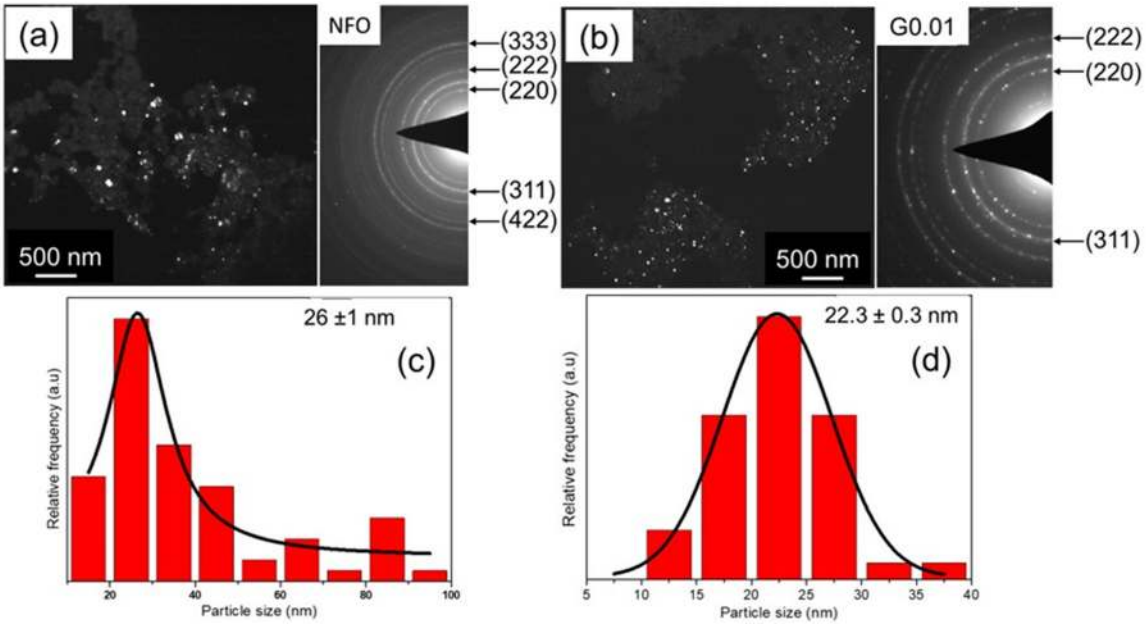

FIG. 3. TEM dark-field micrographs and SAD pattern of (a) NFO and (b) G0.01 as synthesized nanoparticles corresponding to the (220) plane, (c) and (d) correspond to the particles size distribution of NFO and G0.01 nanoparticles, respectively.

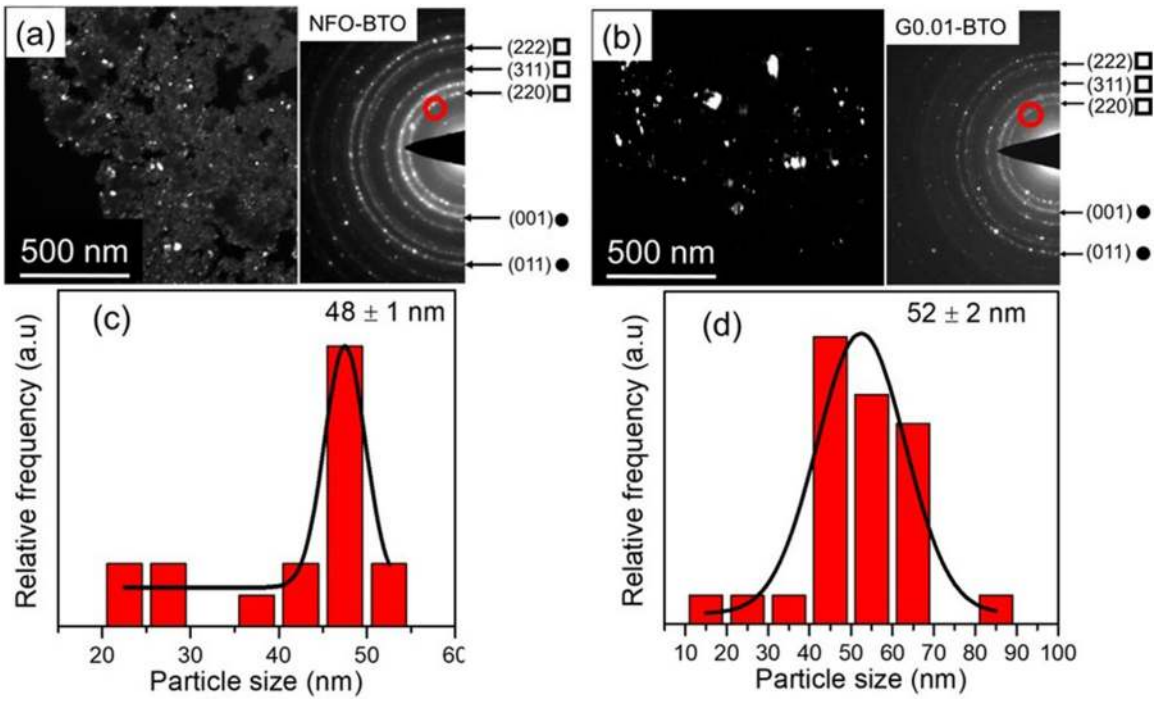

FIG. 4. Dark-field micrograph of nanocomposites indicating the bright crystallites to be of (a) NFO and (b) G0.01 nanoparticles corresponding to (220) planes, (c) and (d) correspond to the particles size distribution of these NFO and G0.01 nanoparticles, respectively, embedded in a BTO shell.

of the nanocomposites were obtained from Rietveld analysis. The phase percentage for NFO is 32 and that of BTO is 68, whereas in G0.01–BTO, they are observed to be 28 and 72 for G0.01 and BTO, respectively. An average crystallite size of 26 nm obtained from TEM matches with the value obtained from XRD indicating the formation of predominantly single crystallite particles as shown in Fig. 3. Dark-field micrographs of nanocomposites of NFO–BTO and G0.01–BTO were captured and are shown, respectively, in Figs. 4(a) and 4(b). The aperture was placed on the (220) peak of NFO and G0.01 to facilitate the observation of the respective crystallites. The crystallite size of NFO calculated from Fig. 4(a) is found out to be 48 (1) nm, whereas for G0.01, it is 52 (2) nm. It is also observed that BTO is not uniformly coated on the irregular surfaces of NFO and G0.01 (due to agglomeration). However, the core–shell structure is retained. Figures 5(a) and 5(b) reveal the presence of Ni, Fe, and Gd in the core (Gd concentration is low, so counts are low as compared to all other elements) and Ba, Ti in the shell.

Magnetization (M) values of NFO and G0.01 nanoparticles are observed to be 38 emu/g and 40 emu/g, respectively, at 60 kOe. In G0.01, Gd^{3+} ions with a magnetic moment of 7.94 μ_B replace Fe^{3+} ions of magnetic moment of 5 μ_B (both from Hund's rules), which leads to an increase in the magnetization of the sample.[20] Rietveld analysis hinted at the preferential substitution of Gd^{3+} in the octahedral site. This fact was further confirmed using Raman spectroscopy analysis as stated in Sec. III. In the spinel system, the moments of the ions at tetrahedral and octahedral sites are antiferromagnetically coupled. The presence of Gd^{3+} at the octahedral site leads to larger magnetic moments of G0.01 nanoparticles compared to the NFO nanoparticles.

In order to obtain an estimate of the anisotropy constant, the M–H data are fitted to the Law of Approach to Saturation (LAS) for cubic anisotropy.[21] In polycrystalline soft magnetic materials,

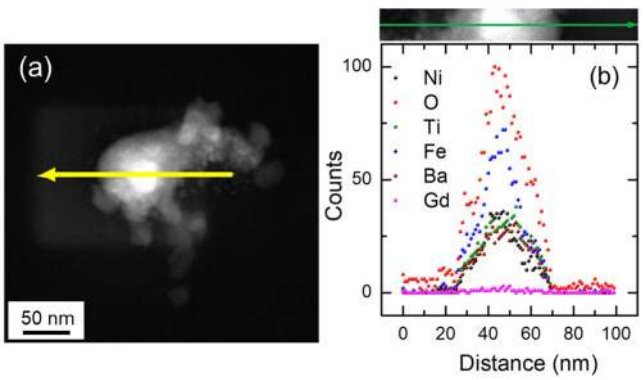

FIG. 5. STEM micrographs of G0.01–BTO nanocomposites. (a) STEM-HAADF image and (b) line profile analysis from left to right suggest that G0.01 is the core and BTO, the shell.[26]

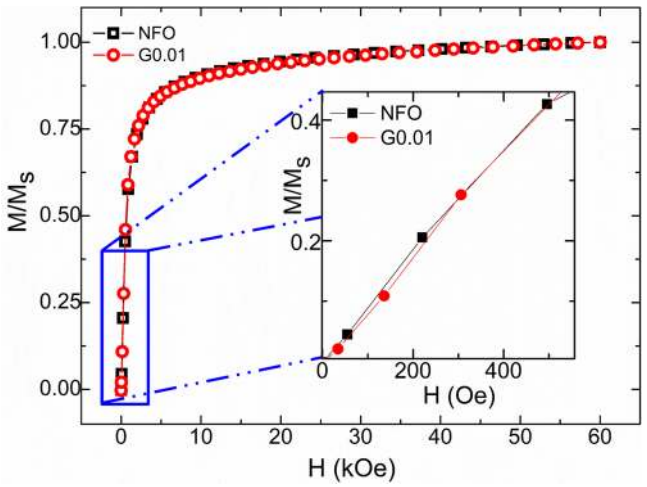

FIG. 6. M/M_s as a function of magnetic field (after subtracting the demagnetizing field).

the LAS is given by

$$M(H) = M_S\left(1 - \frac{a_1}{H} - \frac{a_2}{H^2}\right) + \chi H, \tag{1}$$

where M_S is the spontaneous magnetization, $\frac{a_1}{H}$ is associated with nonmagnetic inclusions and existence of structural defects, $\frac{a_2}{H^2}$ is due to uniform magnetocrystalline anisotropy, and χ is the magnetic susceptibility. The coefficient a_2 for a ferromagnet with a cubic crystal structure is given by

$$a_2 = \frac{8}{105}\frac{K_1^2}{M_S^2}, \tag{2}$$

where K_1 is the cubic anisotropy constant of first order. The estimated value of K_1 of NFO is 2.97×10^4 J/m^3 (reported value is 3.48×10^4 J/m^3),[21] whereas that of G0.01 is 4.99×10^4 J/m^3. The χ values are found to be in the order of 10^{-6}.

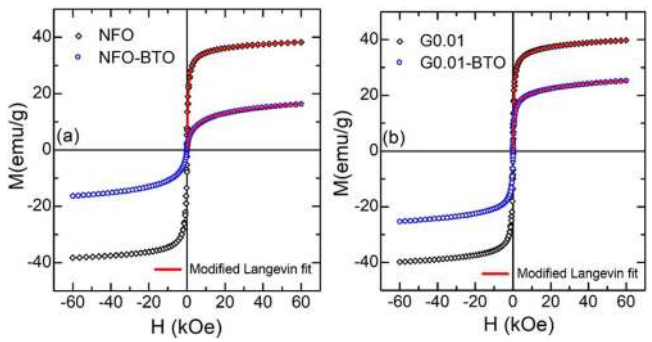

FIG. 7. Langevin fit of the curves (a) NFO, (b) G0.01, (c) NFO–BTO, and (d) G0.01–BTO.

In order to substantiate the values of the anisotropy constants obtained, the magnetization curves, after the demagnetizing fields (assuming spherical particles) were subtracted, were normalized to the respective values at 60 kOe (Fig. 6). From the figure (inset of Fig. 6), it can be seen that there is a crossover at 306 Oe as G0.01 has slightly higher anisotropy as well as higher magnetization compared to NFO.

Magnetization curves of NFO and G0.01 nanoparticles with the nanocomposites NFO–BTO and G0.01–BTO are plotted in Figs. 7(a) and 7(b). The figures indicate superparamagnetic-like behavior in both the nanoparticles and the composites. The curves were fitted to the modified Langevin function

$$M = (1-\alpha)\left[1 - e^{\frac{H}{H_Z}}\right] + \alpha L\left(\frac{\mu H}{k_B T}\right), \tag{3}$$

where μ is the magnetic moment of a single particle and $L(x) = \left[\coth(x) - \frac{1}{x}\right] + \chi_P H$. χ_P is the high field paramagnetic susceptibility. α is the paramagnetic fraction and $\alpha L(x)$ represents the temperature and field dependent paramagnetic fraction of the sample. $(1-\alpha)$ is the ferromagnetic fraction and the moment tends to saturate near $H = H_z$.

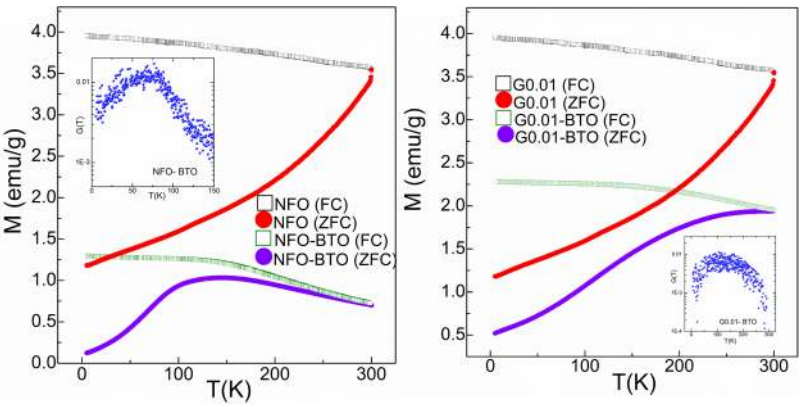

FIG. 8. M–T curves of (a) NFO–BTO and (b) G0.01–BTO.

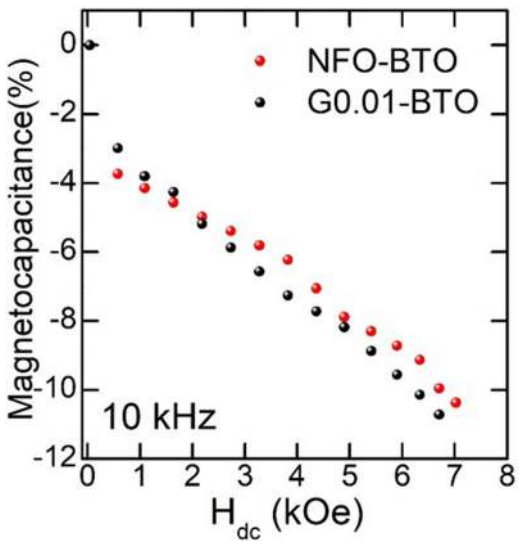

FIG. 9. MC% of NFO–BTO and G0.01–BTO nanocomposites.

First quadrant M–H curves were fitted to Eq. (3). The values of saturation magnetization (M_s) of NFO–BTO and G0.01–BTO nanocomposites are 16 emu/g and 25 emu/g, respectively. Due to the higher magnetization, G0.01 nanoparticles are more agglomerated compared to NFO, which enables them to get entrapped in a BTO shell.

In the present case, $(1-\alpha)$ is attributed to the net magnetic moment of NFO nanoparticles which is 0.7; upon the formation of a composite with a BTO shell, this value is reduced to 0.4. However, in the case of G0.01–BTO, the particles were more agglomerated and the value of 0.7 of $(1-\alpha)$ supports the above. χ_P, the paramagnetic contribution, increases with the addition of the non-magnetic shell and from this it is evident that the inter-particle interaction in the core has decreased. To observe the superparamagnetic effect, temperature dependent magnetization measurements were carried out in field cooled (FC) and zero field cooled (ZFC) modes with 100 Oe as an applied field and the M–T curves are shown in Figs. 8(a) and 8(b).

ZFC and FC curves of NFO-BTO composite meet each other between 250 K and 300 K and those of G0.01–BTO composite at 300 K. The ZFC curves of the composites have inflection points at 71 K (NFO–BTO) and 133 K (G0.01–BTO), whereas those of NFO and G0.01 nanoparticles do not show any inflection. The peak in the ZFC curve is attributed to the hindered spin response of the system below the blocking temperature. There can be either particle size dependent spin blocking mechanism or hindered spin response due to a diamagnetic shell around the ferromagnetic core. $G(T)$ which is defined as[22]

$$G(T) = \frac{d}{dT}\left[M_{FC}(T) - M_{ZFC}(T)\right] \tag{4}$$

confirms that the blocking of spin is due to the diamagnetic shell in the composites as shown in the insets of Figs. 8(a) and 8(b).

Strain generated on the application of a magnetic field is transferred on to the piezoelectric phase, and the potential drop across the sample is measured. Magnetocapacitance (MC) was further determined using the relation given below,

$$\text{MC}\,\% = \frac{C(H) - C(0)}{C(0)} \times 100\%. \tag{5}$$

With the increase in the applied magnetic field, the absolute value of MC decreases, and at higher values of magnetic field, it remains unsaturated. Figure 9 shows the magnetocapacitance (MC%) with a magnetic field up to 7 kOe at a frequency of 10 kHz. The value of MC is found to be −10.2% at 7 kOe for NFO–BTO nanocomposite, whereas, of G0.01–BTO, it is −10.7%.

The polarization arises from the BTO phase, and both NFO and G0.01 exhibit a negative magnetostriction and thus, MC increases in the negative direction with increasing magnetic field.[23] Furthermore, in order to ascertain the magnetoelectric coupling, magnetic field assisted magnetoelectric voltage coefficient for NFO–BTO and G0.01–BTO composites were measured. These core–shell powders were pressed into disks of 6 mm diameter × 1 mm thickness and in-plane (magnetic field in the plane of the disk) and out-of-plane (magnetic field perpendicular to the plane of the disk) measurements were carried out on the sample, by varying ac magnetic field and the corresponding electrical response was recorded

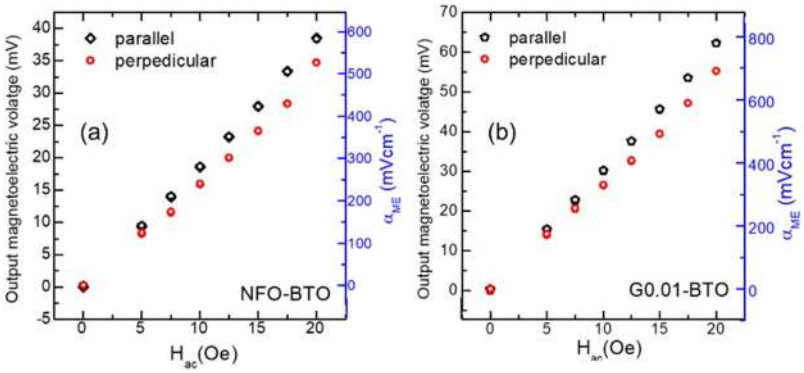

FIG. 10. Variation of output magnetoelectric voltage (mV) and α_{ME} (mV cm^{-1}) of (a) NFO–BTO and (b) G0.01–BTO nanocomposites with the applied ac field.

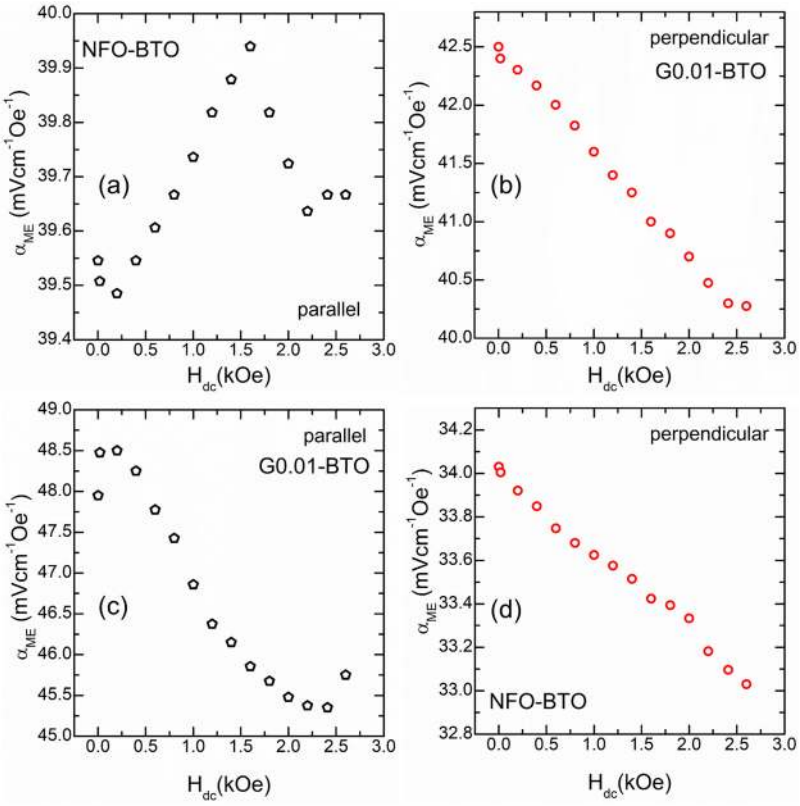

FIG. 11. Variation of magnetoelectric voltage coefficient of (a) NFO–BTO in parallel and (b) perpendicular configuration and (c) G0.01–BTO in parallel and (d) perpendicular configuration.

using a lock-in amplifier.[24] The magnetoelectric voltage coefficient (α_{ME}) was calculated by measuring the voltage (V) drop across the core–shell nanocomposites and using the formula

$$\alpha_{ME} = \frac{1}{t}\left(\frac{dV}{dh}\right), \tag{6}$$

where t represents the thickness of the sample and h denotes the applied ac magnetic field.

Figure 10 shows the variation of output magnetoelectric voltage and α_{ME} with ac magnetic field for both the composites. α_{ME} increases linearly with the applied ac magnetic field in accordance with the literature[24,25] and upon doping with Gd, α_{ME} increases from 570 to 770 mV/cm^{-1}. G0.01 has a higher anisotropy constant (4.99×10^4 J/m^3) as discussed in Sec. III giving rise to a higher α_{ME} value of G0.01–BTO compared to NFO–BTO ($K_1 = 3.48 \times 10^4$ J/m^3). Fixing the ac field at 5 Oe, variations of α_{ME} with dc magnetic field were calculated in parallel as well as perpendicular configuration (Fig. 11). In the parallel configuration, the α_{ME} value obtained for NFO–BTO is 40 mV/cm^{-1} Oe^{-1}, whereas in the perpendicular configuration, it is 49 mV/cm^{-1} Oe^{-1}. In the case of G0.01–BTO, the α_{ME} values, for parallel and perpendicular modes obtained, are 48 and 43 mV/cm^{-1} Oe^{-1}, respectively. The value of α_{ME} obtained in the parallel configuration, for G0.01–BTO is higher than that of NFO-BTO indicating an increase of planar anisotropy compared to the perpendicular anisotropy.

IV. CONCLUSIONS

Nanocomposites of core–shell NFO–BTO and G0.01–BTO were synthesized by the sol-gel technique and were investigated through XRD, magnetization, TEM, MC, and ME measurements. The compounds were found to form in the single phase inverse spinel and a perovskite structure with space group $Fd\bar{3}m$ and $P4mm$, respectively. The particle sizes of the nanoparticles estimated using TEM micrographs were in agreement with the crystallite sizes obtained from XRD. Both G0.01–BTO and NFO–BTO exhibited a negative MC%, which were corroborated with magnetoelectric measurements.

REFERENCES

[1]H. Schmid, Ferroelectrics **162**, 317 (1994).
[2]N. A. Spaldin and M. Fiebig, Science **309**, 391 (2005).
[3]D. Viehland, J. F. Li, Y. Yang, T. Costanzo, A. Yourdkhani, G. Caruntu, P. Zhou, T. Zhang, T. Li, A. Gupta, M. Popov, and G. Srinivasan, J. Appl. Phys. **124**, 061101 (2018).
[4]K. K. Bharathi, K. Balamurugan, P. N. Santhosh, M. Pattabiraman, and G. Markandeyulu, Phys. Rev. B **77**, 172401 (2008).
[5]K. K. Bharathi, J. A. Chelvane, and G. Markandeyulu, J. Magn. Magn. Mater. **321**, 3677 (2009).

[6]J. V. D. Boomgaard, D. R. Terrell, R. A. J. Born, and H. F. J. I. Giller, J. Mater. Sci. **9**, 1705 (1974).
[7]H. Palneedi, V. Annapureddy, S. Priya, and J. Ryu, Actuators **5**, 9 (2016).
[8]D. L. Sekulic, Z. Z. Lazarevic, M. V. Sataric, C. D. Jovalekic, and N. Z. Romcevi, J. Mater. Sci. Mater. Electron. **26**, 1291 (2015).
[9]N. S. Panwar and B. S. Semwal, Ferroelectrics **115**, 1 (1991).
[10]R. Liu, Y. Zhao, R. Huang, Y. Zhao, and H. Zhou, J. Mater. Chem. **20**, 10665 (2010).
[11]K. Raidongia, A. Nag, A. Sundaresan, and C. N. R. Rao, Appl. Phys. Lett. **97**, 062904 (2010).
[12]J. P. Zhou, L. Lv, Q. Liu, Y. X. Zhang, and P. Liu, Sci. Technol. Adv. Mater. **13**, 045001 (2012).
[13]A. Banerjee, J. Zhang, P. Zhou, K. Tuppil, G. Sreenivasulu, H. Qu, T. Zhang, R. Timilsina, F. A. Chavez, and G. Srinivasan, J. Magn. Magn. Mater. **460**, 424 (2018).
[14]A. Chaudhuri and K. Mandal, J. Magn. Magn. Mater. **377**, 441 (2015).
[15]K. K. Bharathi and G. Markandeyulu, J. Appl. Phys. **103**, 07E309 (2008).
[16]S. Mallesh and V. Srinivas, J. Magn. Magn. Mater. **475**, 290 (2019).
[17]S. Betal, M. Dutta, L. F. Cotica, A. S. Bhalla, and R. Guo, Ferroelectrics **503**, 68 (2016).
[18]S. M. Subhani, J. A. Chelvane, and A. Arockiarajan, J. Phys. D Appl. Phys. **51**, 295001 (2018).
[19]G. L. Jadhav, S. D. More, C. M. Kale, and K. M. Jadhav, Phys. B Condens. Matter **555**, 61 (2019).
[20]S. E. Shirsath, R. H. Kadam, S. M. Patange, M. L. Mane, A. Ghasemi, and A. Morisako, Appl. Phys. Lett. **100**, 042407 (2012).
[21]B. K. Chatterjee, C. K. Ghosh, and K. K. Chattopadhyay, J. Appl. Phys. **116**, 153904 (2014).
[22]S. Kuila, S. Tiwary, M. R. Sahoo, A. Barik, P. D. Babu, V. Siruguri, B. Birajdar, and P. N. Vishwakarma, J. Appl. Phys. **123**, 064101 (2018).
[23]K. C. Verma, D. Singh, S. Kumar, and R. K. Kotnala, J. Alloys Compd. **709**, 344 (2017).
[24]P. Kaviraj, R. Pramanik, and A. Arockiarajan, Ceram. Int. **45**, 12344 (2019).
[25]B. R. H. M. Thankachan, A. Mayeen, S. Karthika, S. Vivek, S. S. Nair, S. Thomas, and N. Kalarikkal, J. Alloys Compd. **731**, 288 (2018).
[26]P. Wagener, J. Jakobi, C. Rehbock, V. C. K. Chakravadhanula, C. Thede, U. Wiedwald, M. Bartsch, L. Kienle, and S. Barcikowski, Sci. Rep. **6**, 23352 (2016).